



Biogenic selenium nanoparticles: trace element with promising anti-toxoplasma effect

Fadwa M. Arafa^a, Nermine M. F. H. Mogahed^a, Marwa M. Eltarahony^b and Radwa G. Diab^a

^aDepartment of Medical Parasitology, Faculty of Medicine, Alexandria University, Alexandria, Egypt; ^bEnvironmental Biotechnology Department, Genetic Engineering and Biotechnology Research Institute (GEBRI), City of Scientific Research and Technological Applications (SRTA-City), Universities and Research centers District, Alexandria, Egypt

ABSTRACT

Toxoplasmosis is an opportunistic infection caused by the coccidian *Toxoplasma gondii* which represents a food and water contaminant. The available chemotherapeutic agents for toxoplasmosis are limited and the choice is difficult when considering the side effects. Selenium is an essential trace element. It is naturally found in dietary sources, especially seafood, and cereals. Selenium and selenocompounds showed anti-parasitic effects through antioxidant, immunomodulatory, and anti-inflammatory mechanisms. The present study evaluated the potential efficacy of environmentally benign selenium nanoparticles (SeNPs) against acute toxoplasmosis in a mouse model. SeNPs were fabricated by nanobiofactory *Streptomyces fulvissimus* and characterized by different analytical techniques including, UV-spectrophotometry, transmission electron microscopy, EDX, and XRD. Swiss albino mice were infected with *Toxoplasma* RH strain in a dose of 3500 tachyzoites in 100 µl saline to induce acute toxoplasmosis. Mice were divided into five groups. **Group I:** non-infected, non-treated, **group II:** infected, non-treated, **group III:** non-infected, treated with SeNPs, **group IV:** infected, treated with co-trimoxazole (sulfamethoxazole/trimethoprim) and **group V:** infected, treated with SeNPs. There was a significant increase in survival time in the SeNPs-treated group and minimum parasite count was observed compared to untreated mice in hepatic and splenic impression smears. Scanning electron microscopy showed tachyzoites deformity with multiple depressions and protrusions, while transmission electron microscopy showed excessive vacuolization and lysis of the cytoplasm, especially in the area around the nucleus and the apical complex, together with irregular cell boundary and poorly demarcated cell organelles. The present study demonstrated that the biologically synthesized SeNPs can be a potential natural anti-*Toxoplasma* agent *in vivo*.

KEYWORDS

Toxoplasma gondii; selenium nanoparticles (SeNPs); *Streptomyces fulvissimus*; antioxidant activity

1. Introduction

Toxoplasmosis is an opportunistic infection caused by the coccidian protozoan, *Toxoplasma gondii* (*T. gondii*) [1], where 30% to 50% of the human population is infected [2]. Acute toxoplasmosis in immunocompetent adults can pass unnoticed, and if manifested, only flu-like symptoms and lymphadenopathy are the main manifestations. Severe complications, including seizures, encephalitis, pneumonia, or chorioretinitis, are manifested in individuals with weak immune systems [3]. Human infection occurs through consuming infected raw or undercooked meat containing tissue cysts or ingestion of water or vegetables contaminated with sporulated oocysts. Other routes of transmission include blood transfusion, organ transplantation, and transplacental transmission [4].

The majority of threats to public health in water systems, particularly in developing countries, originate from microbial contaminations which include pathogenic bacteria, viruses, fungi, and parasites [5]. *Toxoplasma gondii* is categorized among such

pathogenic contaminants that are the main causative agents of water-borne diseases, either directly or indirectly via animal feces containing any stage of its life cycle (trophozoites, tissue cysts, or sporulated oocysts) [6].

The available chemotherapeutic agents for the treatment of toxoplasmosis are limited and the choice is even more difficult when considering the side effects. Trimethoprim is the main drug in treating acute disease which targets the folate pathway and DNA synthesis. The drug efficacy was found to be potentiated when combined with sulfonamides. Myelotoxicity that can necessitate the stoppage of therapy is of course a problem, especially in congenitally infected neonates and immunocompromised patients who usually require a prolonged regimen [7]. Moreover, drug resistance to sulfonamides has been documented [8].

Nanotechnology has improved the therapeutic efficiency against several pathogens by enhancing the biological, optical, physicochemical, magnetic, and thermal characteristic features of nanoparticles

[9–11]. Interestingly, the biology-based green routes exhibit numerous merits over physicochemical approaches in a biocompatible, eco-friendly, and cost-effective manner [12]. Wherein, the biological means neglect the use of hazard-reducing chemicals, higher temperature, and higher energy which all required higher cost maintenance and well-trained experts [12]. In biological approaches, the biological entities mediate the synthesis, assembly, and organization of the matters in a nanometer scale. Such biogenic means comprise synthesis by microorganisms and plants. Via phytonanotechnology, different plant organs (e.g. roots, stems, leaves, and fruits) or their extracts were utilized as reducing, stabilizing, and capping agents in the fabrication process. Generally, proteins, organic acids, vitamins, and secondary metabolites (e.g. polyphenols, flavonoids, alkaloids, heterocyclic compounds, terpenoids, and polysaccharides) play a master role in the whole process beginning from metal salt reduction; ending with functionalization of nanoparticles by different functional groups such as hydroxyl groups of polyphenols and carbonyl groups of amino acids [13–15]. On the other hand, the microbial nanofactories symbolize their capability to accumulate and detoxify metal bulk molecules either by bioreduction or biosorption. As reported by [15] the former strategy followed by microbes (e.g. bacteria, fungi, algae) could be implemented through assimilatory chemical reduction [15]. Wherein, the reductase enzymes reduce metal salts to their counterparts of nanoparticles with less polydispersity. Regarding the latter strategy, the metal ions are attracted to the functional groups scattered on the microbial cell wall and conducted the synthesis process of nanoparticles. Accordingly, the microbes mediate intracellular or extracellular fabrication of metal nanostructures. Interestingly, various methods were described for nanoparticles production using live or dead microbial biomass, their extracts, or even derived components (e.g. enzymes, polysaccharides, pigments, etc.) [12,14]. Remarkably, the fabrication of nanoparticles by bacteria, in particular actinomycetes, appeals a great interest due to their superior capacity in metal binding and accumulation and fast propagation, which subsequently provides lower incubation time. Besides, their ability to resist and reduce the high concentration of metals from bulk forms to their nanoforms by multiple and diverse catalyzing and functionalizing biomolecules. In addition, actinomycetes are characterized by their capability to generate new chemical entities, namely secondary metabolites or antibiotics, which could be conjugated with nanoparticles and boost their biological activities [13,16]. Let alone, the easiness of harvesting and higher yield in the production with a narrow size and uniform distribution [17,18].

Metal nanoparticles, such as silver, gold, titanium, copper, iron, and zinc are considered highly targeting and specific drug delivery systems for various therapeutic agents starting from antibiotics up to anticancer drugs. They increase the circulation time for drugs and inhibit rapid renal excretion and reduce the side effects [19,20]. In spite of the easiness to obtain and functionalize, certain metal nanoparticles have drawbacks being non-biodegradable, with the risk of toxicity [21]. Selenium (Se) is an essential trace element that is naturally found in dietary sources especially seafood and cereals [22]. Dietary selenium consumption (55–70 µg per day) has beneficial effects as regards thyroid protection, cardiopulmonary enhancement, and reduced risk of cancer [23].

Se and selenocompounds showed promising antiparasitic effects through antioxidant, immunomodulatory, and anti-inflammatory mechanisms [24], besides their anti-apoptotic effect mainly against protozoan parasites [25]. Sodium selenite and diphenyl diselenide were incorporated into anti-*Toxoplasma* agents and were found to modulate the exacerbated immune response in acute toxoplasmosis [26]. The new scope of utilizing nanocarriers to increase the solubility and bioavailability of the loaded drug is helpful not only in increasing the efficacy of the latter but also in decreasing the side effects and toxicity [27]. Selenium and SeNPs offered hepatoprotective and antioxidant potentials against chronic diseases such as diabetes, cancer, and infectious diseases including parasitic ones such as malaria, leishmaniasis, and chronic toxoplasmosis [28,29]. This is based on their capacity to denature the DNA of the vital organelles, hence, disrupting the membrane permeability and ATP synthesis leading to cell death [30–32].

Accordingly, the present study was carried out to evaluate the potential efficacy of biologically synthesized SeNPs against acute toxoplasmosis in a murine model. Noteworthy, this is the first study to address the biofabrication of SeNPs from a unicellular filamentous bacterium, namely *Streptomyces fulvissimus*. Moreover, this study aims to highlight the therapeutic capacity of this safe, eco-friendly, biologically prepared SeNPs on the virulent RH strain of *Toxoplasma gondii* *in vivo* that goes above and beyond to prove the mechanism of action of this trace element by parasitological, antioxidant, and ultrastructural evidence.

2. Material and methods

2.1. Ethics statement

The experiment was performed following ethical animal guidelines and regulations set by the Ethics Committee of Faculty of Medicine, Alexandria University, Egypt (approval number: 0305021). This is

per the internationally accepted principles for laboratory animal use and care.

2.2. Parasite

RH virulent *T. gondii* strain was maintained in the laboratory in the Medical Parasitology Department, Alexandria Faculty of Medicine, by serial intraperitoneal passages of tachyzoites into Swiss strain albino mice. Peritoneal exudates containing the tachyzoites were collected from previously infected mice and washed in phosphate buffer saline to be used in mice infection. Each mouse was infected by intraperitoneal injection of 3500 tachyzoites in 100 μ l saline [33].

2.3. Preparation and characterization of selenium nanoparticles (SeNPs)

2.3.1. Microorganism separation, cultural conditions, and biosynthesis method

The bacterial strain applied in the current study was screened from a water sample collected from Mariout Lake (Alexandria, Egypt). The bio-nanofactory isolate was identified molecularly by 16S-rDNA, sequenced, and submitted in the GenBank as *Streptomyces fulvissimus* (EM1) under accession number KY964506 [17]. For SeNPs biosynthesis, 10^8 CFU/mL of EM1 was cultivated in nutrient broth media (2 g yeast extract, 5 g peptone, 5 g NaCl, and 1 g Lab-lemco/liter) supplemented by 2 mM of Na_2SeO_3 . The inoculated flasks were incubated at 30°C for 96 h under shaking conditions (150 rpm). In parallel, in two control trials, media with metal precursors lacking bacterial inoculum and media with bacterial inoculum without Na_2SeO_3 were incubated exactly as previously mentioned. The bio-reduction of Na_2SeO_3 and its bio-transformation to SeNPs was monitored visually during the incubation period and inferred through the altering of media and biomass colors. At the end of the incubation period, the biomass containing SeNPs was collected by centrifugation at 11,000 \times g for 20 min and washed several times with double distilled H_2O and 70% ethyl alcohol to eliminate any residuals. The SeNPs were extracted from the cell as the procedure described previously by Eltarahony et al., 2018. Briefly, the microbial pellets were disrupted by suspending them in TSE lysis buffer followed by sonication at 60–80% amplitude for 20 min with a 0.6 s pulse rate. The extracted SeNPs were subjected to characterization techniques after centrifugation, washing, and drying steps [12].

2.3.2. Instrumental characterization of synthesized SeNPs

The optical feature of SeNPs was recorded using UV-Vis double beam spectrophotometer (Labomed model) in the range of 200–800 nm wavelength at room temperature. To visualize the morphology and

size of SeNPs, the transmission electron microscope (TEM- JEOL JEM-1230, Japan) was employed. X-ray diffraction (XRD) of SeNPs was acquired by Bruker MeaSrv (D2–208219) diffractometer in 2θ range from 20° to 90°, at a scanning rate of 0.02 °/sec at 30 kV and 30 mA current. The obtained diffractogram was compared with Joint Committee on Powder Driven Standards (JCPDS). However, the elemental composition of as-prepared NPs was verified by EDX, JEOL JEM-1230, Japan [9]. Further, the functional groups conjugated with SeNPs were detected using Fourier-transform infrared spectroscopy (FT-IR) analysis by Shimadzu FT-IR-8400 S, (Japan). In general, the biogenic SeNPs were blended evenly with KBr and formulated into disks at high pressure, thereby scanned in the region of 4000 to 400 cm^{-1} . Moreover, the size distribution profile of SeNPs in aqueous solution, surface charge, polydispersity index (PDI), and their zeta potential were assessed via zeta sizer (Malvern Instrument ZS-Nano, UK) at a temperature of 25 °C with a scattering angle of 90° [9].

2.4. Drugs

The drug regimen started on the first day post-infection (PI) and continued for seven successive days. Cotrimoxazole (CMX) (sulfamethoxazole/trimethoprim) oral suspension (GlaxoSmithKline, Egypt) was used as a reference drug. It is a combination of sulfamethoxazole and trimethoprim (200/40 mg/5 ml). The cotrimoxazole dose given to mice was calculated according to an equation from the human dose [34]. It was given orally on the same day of infection in a dose of 370 mg/kg divided into two doses for seven successive days [35]. SeNPs administration dose was determined after a pilot study to be 1.5 mg/kg. All those formulae were suspended in 100 μ l saline/dose/mouse and then administered orally by gavage needle from the first day post infection (PI) for six days.

2.5. Animal grouping and study design

Sixty male Swiss strain albino mice, 3–5 weeks old and 20–25 grams weight, were used in the present study. The experimental study followed the international regulations of animal care. Except for the uninfected control mice, each mouse was infected with tachyzoites of the RH strain of *Toxoplasma gondii* in a dose of 3500 tachyzoites in 100 μ l saline by intraperitoneal injection. Mice were divided into five groups, 12 mice each:

Group I: normal non-infected, non-treated.

Group II: RH -infected, non-treated group.

Group III: non-infected, treated with SeNPs.

Group IV: infected, treated with CMX.

Group V: infected, treated with SeNPs.

Six mice from each subgroup were sacrificed on the eighth day PI. The remaining mice were observed for their survival till the end of the experiment.

2.6. Assessment of anti-Toxoplasma effect

2.6.1. Parasitological study

2.6.1.1. Survival time. Mice from all groups were observed daily to determine the survival time till the end of the experiment. Kaplan–Meier survival curve was used for daily observation of mice (6 mice/each studied group) for 15 days to determine the percentage of mice living over time [36].

2.6.1.2. Impression smears for parasite burden estimation. Impression smears were prepared from the liver and spleen of all infected mice, stained with Giemsa, and tachyzoites were counted in each smear in 10 oil immersion fields. The mean number of tachyzoites of 10 different oil immersion fields from each studied organ of each mouse was calculated then that of the group was determined [37].

2.6.1.3. Ultrastructural study. *Toxoplasma* tachyzoites were collected from the peritoneal wash of infected mice in all studied groups. Tachyzoites suspensions were fixed in glutaraldehyde for further scanning and transmission electron microscopic examination [38,39].

2.7. Biochemical study

Sera were collected from all sacrificed mice on the 7th day PI to assess the total antioxidant capacity (TAC) [40]. It was performed to measure the antioxidant status of liver homogenate prepared from mice in all groups using the Total Antioxidant Capacity (TAC) Colorimetric Assay Kit (biodiagnostic, Egypt). It is based on the principle that the antioxidants present in the sample eliminate a certain amount of the provided hydrogen peroxide (H₂O₂). Then, the residual H₂O₂ is determined colorimetrically by an enzymatic reaction which involves the conversion to a colored product [41].

2.8. Statistical analysis of the data

Data were fed to the computer and analyzed using IBM SPSS software package version 20.0. (Armonk, NY: IBM Corp). Kolmogorov–Smirnov was used to verify the normality of the distribution of variables. ANOVA was used for comparing the different studied groups followed by Post Hoc test (Tukey) for pairwise comparison. Kaplan–Meier Survival curve was used for the significant relation with overall survival. The significance of the obtained results was judged at the 5% level.

3. Results

3.1. Characterization of prepared SeNPs

Initially, the bioproduction of SeNPs was evidenced via alteration in the color of EM1 cells and the surrounding aqueous medium from yellow to red. Whereas, the color of control trials remained constant without any change; implying the bioreduction of sodium selenite to SeNPs. By UV-visible spectroscopic examination of the optical properties of biosynthesized SeNPs, the latter exhibited a characteristic absorption peak in the range of 260–280 nm (Figure 1a). Besides, another minor peak with slight intensity was also observed in the rejoin of 500–600 nm [42,43]. Thereafter, the elemental analysis of examined SeNPs samples, via EDX, confirmed a strong presence of Se at 1.7, 11.3, and 12.4 keV with a maximum weight of 76.92%, along with C at 0.27 keV with a maximum weight of 23% (Figure 1b). Additionally, the phase identity, purity, and crystalline nature of as-prepared SeNPs was verified by X-ray diffractogram (Figure 1c). As observed, a series of characteristic peaks were displayed at $2\theta = 29.7^\circ, 45.4^\circ, 51.5^\circ, 55.6^\circ,$ and 65.3° which correspond to (101), (111), (201), (003), and (210) Bragg's reflection, respectively were detected. These diffraction peaks were well synchronized with the standard spectrum (JCPDS, number 42–1425). Furthermore, TEM micrographs, as depicted in Figure 1(d), showed SeNPs biosynthesized by EM1 as numerous uniform spherical NPs with particle size ranging from $2\text{--}10 \pm 0.7$ nm and well scattered without obvious aggregation. In addition, as a noninvasive technique, Dynamic Light Scattering (DLS) was employed to define SeNPs surface charge, stability and hydrodynamic diameter as well. This technique unveiled the presence of Brownian motion among SeNPs in a colloidal solution; thus, indicating the homogeneous distribution of the particles in monodispersity and without agglutination, which eventually participates in long-term stability. As represented in Figure 1(e), the particle size distribution curve of SeNPs signified that 78% of SeNPs were assessed by 74.8 nm with a standard deviation of 25.1%, besides, $11.9 \pm 2.1\%$ of them recorded 10.9 nm. Whereas, other particles in the colloidal solution were assessed by 527.3 nm ($13.3 \pm 4.9\%$). On the other hand, the polydispersity index (PDI) was evaluated as 0.355 and the electrokinetic potential of bacterially synthesized SeNPs (ζ -potential) recorded was -33.7 mV (Figure 1f).

Interestingly, FTIR analysis was employed to scrutinize the bonding chemical groups associated with streptogenic SeNPs of the present study. As depicted in (Figure 1g), some intensive bands were notably distinguished in the FTIR spectrum of the as-prepared SeNPs. Initially, the spectral bands at 3266 and 3069 cm^{-1} were assigned to O–H groups of the water molecule adsorbed physically on SeNPs [44]. Whereas, the

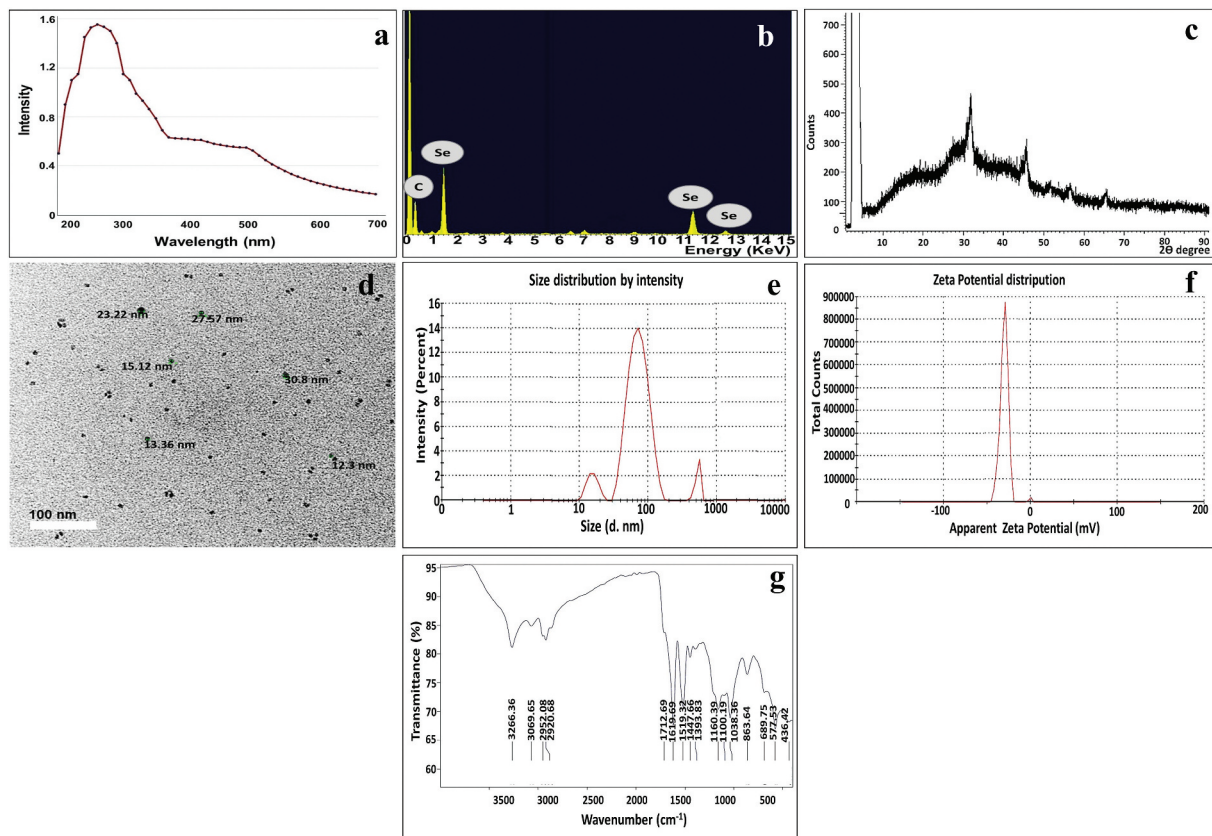


Figure 1. Structural and morphological properties of biosynthesized SeNPs: (a)u.V-Vis, (b)edx, (c)xrd and (d)tem, (e)dls, (f) ζ -potential and (g) FT-IR.

vibration bands at 2952 and 2920 cm^{-1} were assigned to the stretching vibration of C-H related to methylene groups of the protein or lipids [9,45]. Meanwhile, the wave numbers of 1712 and 1619 cm^{-1} were attributed to carboxylate COO stretching vibration and amide-I/amide-II linkages as stated by Qi et al. [46], and Jyoti et al. [47], respectively. However, the absorption peaks at 1519 and 1447 cm^{-1} were related to Amide I/II groups and C=O of carboxylic acid, correspondingly. More so, the spectral band at 1393 cm^{-1} could be assigned to C-N of aromatic amino groups or carboxyl groups (-COOH) [48,49]. Interestingly, the spectral bands in the region of 1200–900 cm^{-1} indicated the occurrence of stretching vibration of PO_4^{3-} , C – O–C, and C – OH groups as reported by Lian et al. [50]. Remarkably, Tugarova et al. [51] demonstrated that polysaccharide groups are allocated within vibration region of 1200–1000 cm^{-1} . Additionally, the spectral bands in the region of 400–700 cm^{-1} symbolized the presence of the metal-oxygen group [52,53]. Noteworthy mentioning that, Al Jahdaly et al. [54] demonstrated the interaction of Se with the hydroxyl group, such as Se-O, could be detected at 570 cm^{-1} , which agreed with our finding.

3.2. Estimation of parasite burden

Infected mice treated with SeNPs (group V) had the minimum parasite count compared to untreated mice

(group III) and CMX-treated group IV, as shown in hepatic and splenic impression smears. Results are shown in Table 1.

3.3. Determination of total antioxidant capacity (TAC)

Assessment of the TAC in sera of studied groups showed the highest values in non-infected groups I and II with no significant difference between them. TAC decreased significantly in all infected groups compared to non-infected ones. Infected non-treated group III and infected, CMX-treated group IV showed significant lowering of the TAC compared to non-infected groups I and II, and when compared to infected, SeNPs-treated group V. The latter group also had a slightly significant hindering of TAC compared to non-infected groups. Results are shown in Table 2.

3.4. Estimation of the survival time

The survival time was assessed for 15 days and there was a high statistically significant difference in mice survival between all studied groups ($p < 0.001$), where all non-infected mice survived till the end of the experiment, whereas infected untreated mice showed a mean survival time of 7.33 days. Regarding treated mice, they flaunted a mean survival time ranging between 9.50 and 11.50

Table 1. Comparison between the different studied groups according to parasite burden in liver and spleen impression smears.

Tachyzoite count	Group III (n = 6)	Group IV (n = 6)	Group V (n = 6)	F	p
In liver impression smear					
Mean ± SD.	3.1 ± 0.4	0.9 ± 0.3	0.7 ± 0.4	73.134*	<0.001*
Median (Min. – Max.)	3.1 (2.4–3.5)	0.9 (0.5–1.2)	0.7 (0.2–1.2)		
Sig. bet. gps.	$p_1 < 0.001^*$, $p_2 < 0.001^*$, $p_3 = 0.773$				
In spleen impression smear					
Mean ± SD.	1.4 ± 0.4	1 ± 0.4	0.4 ± 0.2	13.983*	<0.001*
Median (Min. – Max.)	1.4 (1–1.8)	1 (0.4–1.5)	0.4 (0.1–0.6)		
Sig. bet. gps.	$p_1 = 0.153$, $p_2 < 0.001^*$, $p_3 = 0.014^*$				

SD: Standard deviation.

F: F for ANOVA test, Pair-wise comparison bet. each 2 groups, was done using Post Hoc Test (Tukey).

p: p- value for comparing between the studied groups.

p1: p- value for comparing between Group III and Group IV.

p2: p- value for comparing between Group III and Group V.

p3: p- value for comparing between Group IV and Group V.

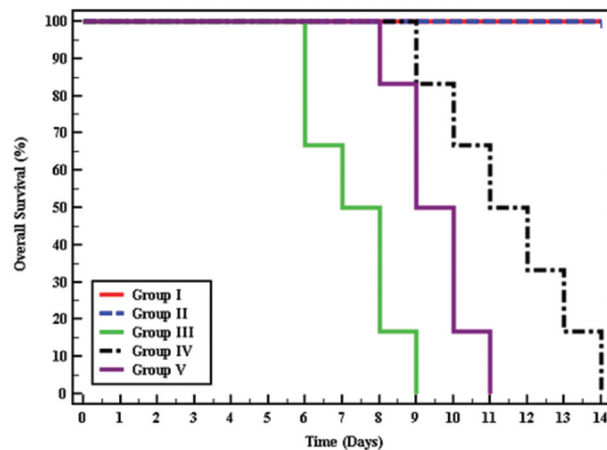
*: Statistically significant at $p \leq 0.05$.**Table 2.** Comparison between the different studied groups according to total antioxidant capacity (TAC).

	Group I (n = 6)	Group II (n = 6)	Group III (n = 6)	Group IV (n = 6)	Group V (n = 6)	F	p
Total antioxidant capacity (TAC)							
Mean ± SD.	1.62 ± 0.06	1.63 ± 0.02	1.28 ± 0.05	1.48 ± 0.04	1.53 ± 0.07	49.515*	<0.001*
Median (Min. – Max.)	1.62 (1.53–1.69)	1.63 (1.60–1.65)	1.29 (1.21–1.34)	1.48 (1.43–1.53)	1.54 (1.43–1.60)		
p ₀		1.000	<0.001*	<0.001*	0.029*		
p ₁			<0.001*	<0.001*	0.019*		
Sig. bet. grps.	$p_2 < 0.001^*$, $p_3 < 0.001^*$, $p_4 = 0.349$						

SD: Standard deviation.

F: F for ANOVA test, Pair-wise comparison bet. each 2 groups, was done using Post Hoc Test (Tukey).

p: p-value for comparing between the studied groups.

p₀: p-value for comparing between Group I and each other group.p₁: p- value for comparing between Group II and each other group.p₂: p- value for comparing between Group III and Group IV.p₃: p- value for comparing between Group III and Group V.p₄: p- value for comparing between Group IV and Group V.*: Statistically significant at $p \leq 0.05$.**Figure 2.** Kaplan-Meier survival curve for overall survival in different groups.

days. The most extended survival time was observed among mice receiving cotrimoxazole (Figure 2).

3.5. Ultrastructure study

3.5.1. Scanning electron microscope (SEM)

In an attempt to explore the effect of treatment on *T. gondii* tachyzoites, an ultrastructural study was

conducted. SEM of tachyzoites obtained from non-treated group III showed uniformly crescentic morphology with a rounded pole and a nearly pointed pole. The site of the conoid was marked at the pointed side by a compressed spring (Figure 3a). In the CMX-treated group (group IV), tachyzoites were severely deformed with excessive irregularities, multiple depressions, and protrusions and the site of the conoid was unremarkable. Some tachyzoites showed completely disrupted morphology with the formation of a dolphin-like structure formed by the combination of deep erosions, several large protrusions, and leakage of internal contents (Figure 3(b,c)). On the other hand, tachyzoites treated with SeNPs (group IV) had a rough surface with minute depressions and multiple protrusions (Figure 4a). The surface was also covered with nanosized deposits ranging in size from 19.61 to 26.95 nm (Figure 4b). Some tachyzoites were deformed with reduced size and evident multiple surface flagella-like projections (Figure 4(c,d)).

3.5.2. Transmission electron microscope (TEM)

Because of the promising parasitological and SEM results, TEM was performed to understand the

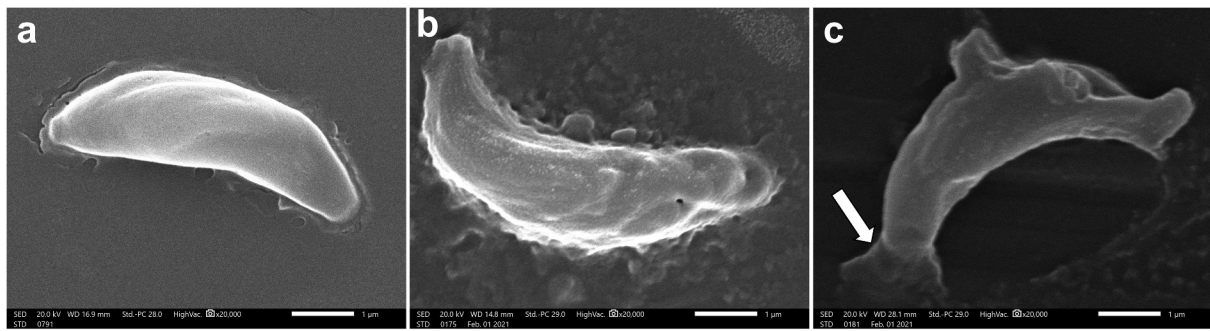


Figure 3. Scanning electron microscopic (SEM) images of. a. Uniformly crescentic normal, non-treated tachyzoite with a rounded pole and a nearly pointed pole. The site of the conoid was marked at the pointed side by a compressed spring (x20000). b. CMX-treated tachyzoite showing surface irregularities with multiple depressions and protrusions (x20000). c. CMX-treated tachyzoite showing completely disrupted morphology with the formation of a dolphin-like structure formed by the combination of deep erosions, several large protrusions, and leakage of internal contents from one end (arrow). The site of the conoid was unremarkable (x20000).

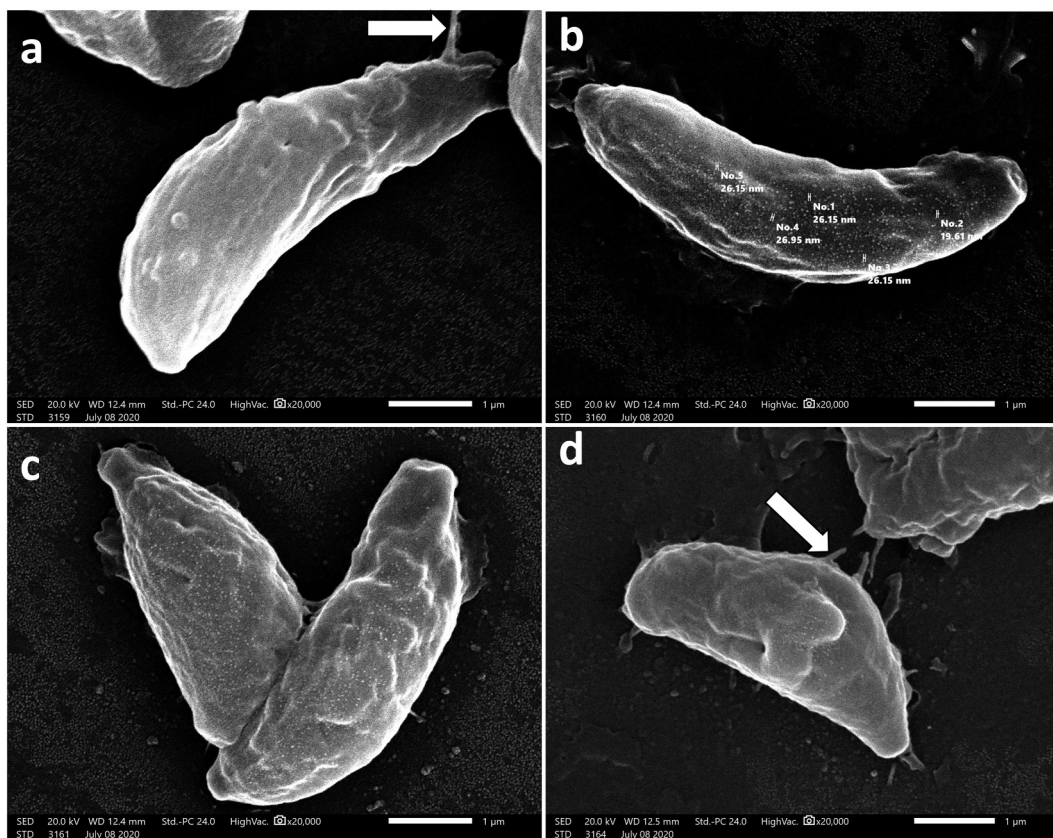


Figure 4. SEM images of SeNPs treated tachyzoites showing. a. Rough surface with minute depressions and multiple protrusions which may form flagella-like projections (arrow) (x20000). b. Rough surface covered with nanosized deposits (size range between 19.61 and 26.95 nm) (x20000). c, d: Reduction in size of some tachyzoites with evident multiple surface depressions and flagella-like projections (arrow) (x20000).

underlying mechanisms. Non-treated tachyzoites were crescent-shaped with intact plasma membrane, apical complex, and nucleus. The conoid, rhoptries, micronemes, dense granules, and lipid bodies also appeared inside the tachyzoites (Figure 5a). The intracellular tachyzoites were surrounded by an intact tubulovesicular network (TVN) inside the narrow-spaced parasitophorous vacuole (PV). Host cell mitochondria and endoplasmic reticulum were recruited around the PV (Figure 5b). While the CMX-treated tachyzoites showed

hazy cytoplasmic membrane, irregular fading nuclear membrane, and disrupted apical complex (Figure 5c).

On the other hand, the SeNPs treated group showed the most extensive and marked morphological and structural changes in the form of destabilization of the PV membrane with leakage of its contents into the cytoplasm of the host cell. In addition, disrupted tachyzoites morphology with vacuolated cytoplasm and flagella-like membrane protrusions were noticed together with irregular cell boundary and poorly

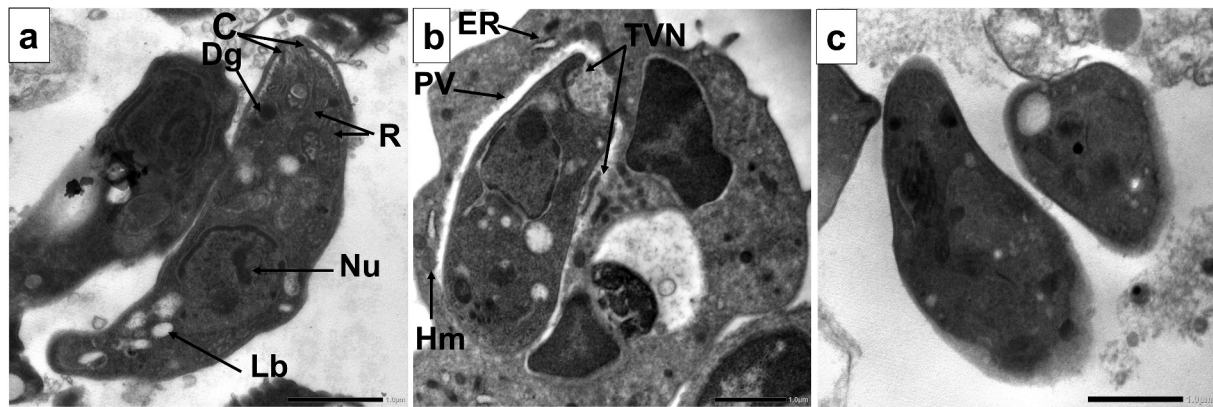


Figure 5. Transmission electron microscopic (TEM) images of. a. Longitudinal section of a normal, non-treated crescent-shaped extracellular tachyzoite having intact plasma membrane with intact apical complex with conoid (C), rhoptries (R). Dense granules (Dg) and lipid bodies (Lb) were present. The nucleus contains two nuclei with an interrupted nuclear membrane denoting nuclear division (x8000). b. Longitudinal section of a normal, non-treated crescent-shaped intracellular tachyzoite with host mitochondria (Hm) and endoplasmic reticulum (ER) in close association with the parasitophorous vacuole (PV). Intact tubulovesicular network (TVN) inside the narrow-spaced PV (x6000). c. CMX-treated tachyzoite showing hazy cytoplasmic membrane, irregular fading nuclear membrane, and disrupted apical complex (x8000).

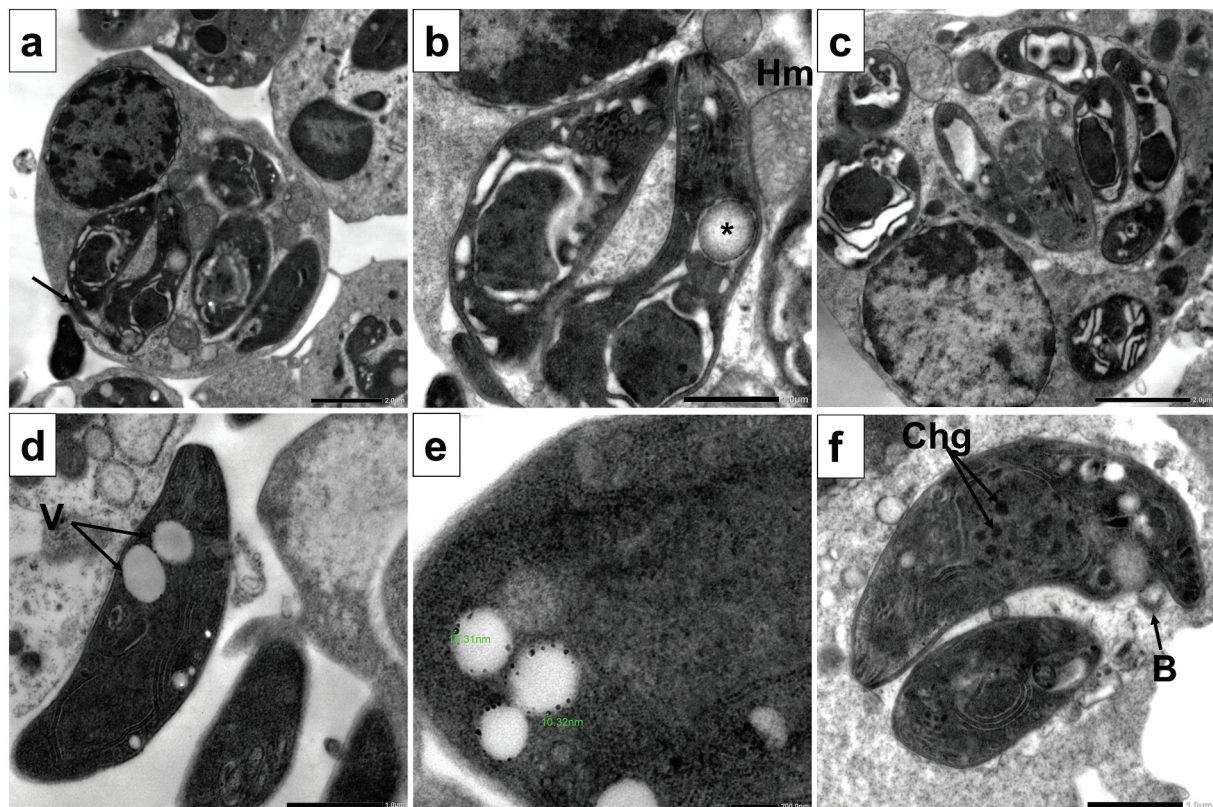


Figure 6. TEM images of SeNPs treated tachyzoites showing. a. Destabilization of PV membrane with leakage of its contents into the cytoplasm of the host cell. Disrupted tachyzoites morphology with vacuolated cytoplasm and flagella-like membrane protrusion (arrow) (x3000). b. With higher magnification, the degenerated nuclear membrane of tachyzoites with absence of nucleolus and halo mark around the nucleus were evident. Also disrupted apical complex and appearance of autophagy vesicles containing materials in different stages of degradation were seen (asterisk). tachyzoites showed extensive clefts and close association with host mitochondria (Hm) (x8000). c. Disruption of PV membrane with leakage of its content into the cytoplasm of the host cell. Multiple tachyzoites showing signs of degradation with extensive cytoplasmic clefts and vacuoles (x4000). d. Extracellular tachyzoites with multiple vacuoles (V) containing nanosized particles (x8000). e. With higher magnification, the particle size is between 10.32 and 16.31 nm (x20000). f. Tachyzoite showing membrane blebs (B), disrupted nuclear membrane with multiple dense chromatin granules (Chg) inside the nucleus. The PV space was widened with disintegrated contents (x8000).

demarcated cell organelles (Figure 6a). Degenerated nuclear membrane of tachyzoites with the absence of nucleolus and halo mark around the nucleus were evident. Also disrupted apical complex and the appearance of autophagy vesicles containing materials in different stages of degradation were seen. Moreover, tachyzoites showed signs of degradation with extensive clefts and vacuoles. Disruption of PV membrane with leakage of its content into the cytoplasm of the host cell and close association with host mitochondria (Figure 6(b,c)). Extracellular tachyzoites showed multiple vacuoles containing nanosized particles. With higher magnification, the particle size ranged between 10.32 and 16.31 nm (Figure 6(d,e)). Tachyzoites showed membrane blebs and disrupted nuclear membrane with multiple dense chromatin granules inside the nucleus. The PV space was widened with disintegrated contents (Figure 6f).

4. Discussion

Treatment of parasitic infection is challenging, not only because of the complicated pathogenesis of the parasitic agent but also due to drug side effects and the emergence of drug resistance. The primary treatment of toxoplasmosis depends on several antibacterial agents mainly sulfadiazine, trimethoprim, spiramycin, and clindamycin, or by repositioning of antimalarial drugs such as pyrimethamine and atovaquone [55]. The main target for these chemotherapeutic agents is the tachyzoite stage of the parasite, however, noncompliance is inevitable due to their numerous side effects [56]. The well-known, widely used anti-*Toxoplasma* agent is the trimethoprim-sulfamethoxazole combination which competitively inhibits the synthesis of folic acid, hence, finally inhibits the parasite DNA and protein synthesis [57]. However, treatment isn't only about killing the parasite, but it extends to counteract the pathology and tissue damage suffered by the host. It is well-known that oxidative stress with oxidant-antioxidant imbalance plays important role in the course of *T.gondii* infection [58]. Therefore, a biogenically synthesized natural antioxidant such as Se in nanoparticle formulation may offer a viable alternative to the traditional anti-*Toxoplasma* chemotherapeutic agents.

Owing to nanotechnology, the interaction between parasites and antiparasitic-loaded nanoparticles has been improved as the penetration of therapeutic agents into the host cells is enhanced by the large surface-volume ratio of nanoparticles [59]. In the present study, the synthesis of biogenic SeNPs was successfully implemented; indicated by the appearance of red color, which was attributed to the excitation of surface plasmon vibrations (SPR) of Se. It is noteworthy that the SPR band deems being special and unique property for materials with metallic nature and UV-Vis

spectroscopy is a ubiquitous tool for its study [60]. In agreement with our results [61]; Vahdati and Tohidi Moghadam [62] and Cittrarasu et al. [63] found the same results for SeNPs synthesized by wet chemical, hydrothermal, and green synthesis approaches, respectively. Additionally, the presence of another minor peak at the range of 500–600 nm could be attributed to some secondary metabolites and other bacterial biomolecules associated with SeNPs; implying their role in the functionalization of the biosynthesized SeNPs. Similarly, other recent studies recorded this observation during the biosynthesis of metal-NPs [42,43].

However, the conjugation of carbon with SeNPs, as highlighted by EDX, could be assigned to the association of SeNPs with microbial organic biomolecules, which is deemed advantageous. This is because the presence of biomolecules provided functionality and stability to the as-prepared NPs [64]. Interestingly, Ur Rahman et al. [65] previously recorded such observation in green synthesized NPs. On the other hand, the phase identity, purity, and crystalline nature of as-prepared SeNPs were verified by X-ray diffractogram which was coincident with the results of Cittrarasu et al. [63]. Whereas Geoffrion et al. [66] and Filipovic et al. [67] prepared SeNPs with amorphous nature. Furthermore, TEM micrographs visualized the morphology and size of SeNPs which depicted small spherical nanoparticles that could invade and penetrate walls of tissues as long as lower than 80 nm [68]. Strikingly, the variation between TEM and DLS results regarding the size of SeNPs could be attributed to the association of bacterial biomolecules with SeNPs. Also as revealed by Venditti et al. [69], the DLS technique determines the overall size of NPs surrounded by an aqueous layer. Similarly, the exact observation was detected previously by other studies [9,12,18]. Meanwhile, the value of PDI revealed a remarkable monodispersity of SeNPs, where small SeNPs diffused rapidly in light scattering intensity by the virtue of repulsive forces between adjacent NPs; therefore, higher stability than non-uniform shapes with larger size particles.

Moreover, the value of ζ -potential, which was assessed by -33.7 mV, pointed out high electrostatic interaction and so, long-term stability in homogenous distribution without further flocculation or sedimentation. It is worth mentioning that the acceptable stability range of ζ -potential values is ± 30 mV, for any particles, where the particles with ζ -potentials more positive or more negative than 30 mV display distinctive stability as stated by Saeb et al. [70]. Additionally, the negative charge of SeNPs could be interpreted by their conjugation with negatively charged streptogenic biomolecules like nucleic acid moieties, proteins, and other secondary metabolites. Apparently, the association of these biological entities with SeNPs

deemed being advantageous, which could be ascribed to their role in providing stability and functionality by mediating as capping and functionalizing agents. Remarkably, overall DLS results of bacterially prepared SeNPs in the current study exhibited better results than other related literature [62,71,72].

Besides, according to the FTIR results, it is obviously emphasizing the conjugation of SeNPs with various functional groups including PO_4^{3-} , amide, $-\text{OH}$, C-H , and $-\text{COOH}$, which are bacterially derived from secondary metabolites, proteins, lipids, and polysaccharides. Interestingly, such bioactive molecules involved in the whole process of SeNPs synthesis beginning from sodium selenite reduction to form the nuclei of Se; passing through the coalesce of the generated nuclei into larger size particles and ending with their stabilization via coating and capping of the particles' surface, which eventually boost the antiparasitic activity easily and efficiently. Likewise, the finding of Ren et al. [73] corresponds to our results.

The World Health Organization (WHO) has made a recommendation on the dose of selenium for adults to be 30 to 40 $\mu\text{g}/\text{day}$ and stated that daily intake of up to 400 μg selenium shall be considered safe [74]. Although Se is considered an essential antioxidant, it is a double-sword element as overdose can lead to the formation of ROS, with subsequent DNA damage, apoptosis, cytotoxicity, and carcinogenesis [75,76]. Hence, dose calculation is an essential step for recruiting the benefits of Se without toxicity dangers. In the present study, the used SeNPs regimen was previously tested and was proved safe in the murine model according to toxicity profile assay [31].

The results of the current work showed a significant lowering effect on the parasite load for SeNPs when compared to non-treated control and CMX-treated groups in splenic impression smears. Selenium can modulate the host's immune response and combat oxidative stress through the antioxidant defense, redox signaling, and homeostasis [77].

The hallmark of toxoplasmosis is a Th1 response evidenced by $\text{IFN-}\gamma$ and $\text{TNF-}\alpha$, which play an important role in controlling tachyzoite replication throughout the infection [78]. Studies revealed that the innate and adaptive immune responses against infectious agents including parasites rely on Se whose deficiency can damage both types of immune responses and, hence, encourages several infections. SeNPs were proved to increase the immunomodulatory cytokines such as IL-12, and $\text{IFN-}\gamma$, which are hallmarks of the Th1 immune response, typical of intracellular infections such as toxoplasmosis [1]. The immunomodulatory effects of selenocompounds can be explained by their suppressive control on lipid peroxidation [26]. On this basis, SeNPs significantly reduced the number of *T. gondii* tissue cysts and controlled the infection in mice as documented by Keyhani et al. [31]. Se

supplementation can maintain T-cell maturation, functions, and T-cell-dependent antibody production thus maintaining the immune response during the course of parasitic infections [79]. Both experimental and human studies showed that Se supplementation has a magnificent immune-stimulant effect on the proliferation of T lymphocytes especially T-helper 1 response, and natural killer cell activity [80–82].

In the present study, it was noticed that statistically insignificant low parasite load was detected in hepatic tissues between CMX and SeNPs-treated groups IV and V. This may be due to higher SeNPs uptake by the spleen compared to the liver cells, hence a significant parasite load reduction was observed in splenic impression smears from SeNPs-treated group. The liver constitutes the main organ of Se uptake after absorption from the intestine and it is the main store for Se in the body, especially in case of Se deficiency. In acute infections, Se supplements after absorption and arrival in the liver will be changed into an intermediate compound Sepp1 which is released from the liver into the plasma to be distributed to different organs for selenoprotein synthesis. This is accomplished by allocation onto apolipoprotein E-receptor-2 whose expression is minimal in the liver and kidney, moderate in the spleen, and higher in other tissues. Thus, it seems that under stressful conditions, as in acute toxoplasmosis, the liver sacrifices its Se content to extrahepatic tissues [83].

Assessment of the TAC in the sera of studied groups revealed the highest values in non-infected groups I and II. While the TAC decreased significantly in all infected groups compared to non-infected ones, SeNPs-treated group V had a slight hindering of TAC compared to non-infected groups with a noticeable shift toward the normal levels. This was expected owing to the influence of Se on the antioxidant enzymatic activity as it was recognized to be a constituent of several glutathione peroxidases [84]. Immediately after host cell penetration, tachyzoites multiply rapidly leading to host cell death with subsequent recruitment of inflammatory cells, mainly lymphocytes, and monocytes. The release of reactive oxygen species (ROS) is a hallmark of the immune response against intracellular parasites. Tachyzoites are a very susceptible stage to this oxidative stress which can cause intracellular parasite death. However, the parasite has its own protective antioxidant system, constituting an *in vivo* virulence factor, with the subsequent expression of parasite superoxide dismutase and catalases, together with the antioxidant role of the parasite thioredoxin and glutathione which are activated to decrease the intracellular concentration of ROS and repair the damaged DNA and proteins. The time when the parasite succeeds to maintain its favorable oxidant-antioxidant balance and control its replicative capacity gives chance for tachyzoites' transformation into

bradyzoites inside the tissue cysts away from the immune response [85,86]. On the other hand, the immune response against the replicating tachyzoites together with the consecutive increase in production of ROS constitute a double sword effect that combats the parasite, but at the same time causes the host's tissue damage [87]. Thus, antioxidant mechanisms start to act, but as they struggle, subsequent depletion of glutathione will occur with redox imbalance and finally, with the establishment of infection, will cause oxidative stress and tissue pathology [88]. Selenium was documented to be a component of several glutathione peroxidases which are considered selenium-containing proteins, or selenoproteins [84]. Additionally, it was found that antioxidant supplementation with vitamins A, C, and E causes enhancement of the redox balance during infection [89]. This antioxidant enhancement was proved to be effective when phenyl diselenide-enriched trimethoprim-sulfamethoxazole was used against chronic toxoplasmosis [88].

Immune responses and inflammatory processes are closely related to oxidative stress, the production of ROS, and redox control processes. Thus, Se through its redox control effect can influence the immune response as was proved by the effect of Se depletion on cytokines profile in mice in viral infections [90,91]. Due to its effect on the integrity of glutathione peroxidases, Se deficiency was found to suppress signaling pathways that activate neutrophils for microbial killing [92,93].

Additionally, the overall survival was noticeably extended among treated mice compared to infected untreated mice. Although the most extended survival time was observed among mice receiving cotrimoxazole, SeNPs succeeded in prolonging the survival time owing to their effects on the immune system and antioxidant defense mechanisms. These effects were confirmed by the ultrastructural alterations noticed by SEM and TEM.

Surface distortion of tachyzoites collected from both treated groups, as shown in scanning electron micrographs, could be due to alteration in the subpellicular cytoskeleton as the shape and the dynamic properties of tachyzoites depend primarily on the cortical cytoskeleton and subpellicular microtubules. In the SeNPs-treated group, the surface changes could be caused by nano-sized particles attacking the parasite surface. Additionally, any deformity in the apical region could be an indication of the efficiency of the tested compound on the tachyzoites invasion capability as the organelles in the apical region are responsible for the entry of the organism into the host cells and in turn causing their multiplication and proliferation [94–96]. These changes could explain the loss of the invasive power and intracellular proliferation capacity of the treated tachyzoites which consequentially

caused the decrease in parasite burden with the increase in the survival time of the treated mice [97].

The effect of CMX was more pronounced and led to complete morphological distortion with the formation of a dolphin-like parasite as shown in the present work. This could be attributed to its ability to cause overexpression of an endogenous SAS6-I protein that forms prominent filaments extending from any part of the tachyzoite [98]. Although the appearance of flagella or filament-like structures has been particularly linked with CMX treatment [97], these changes were also observed in SeNPs treated group which suggests a similar underlying mechanism of action.

As regards TEM results, the non-treated tachyzoites maintained their characteristic crescent shape with intact plasma membrane, apical complex, and nucleus. The intracellular tachyzoites were surrounded by an intact tubulovesicular network (TVN) inside the narrow-spaced PV where they employed the host cell machinery such as mitochondria and endoplasmic reticulum for their benefits. Meanwhile, the CMX-treated tachyzoites showed a hazy cytoplasmic membrane, irregular fading nuclear membrane, and disrupted apical complex. This could be explained by the fact that CMX is an anti-folate drug thus it interferes with the folic acid cycle and DNA synthesis [99]. Anti-folates can inhibit parasite cell division, DNA/RNA production, and protein synthesis which may lead to these morphological alterations [97]. This goes hand in hand with the results of Gaafar et al. [100] and could be ascribed to the ability of CMX to upregulate the expression of an endogenous SAS6-I protein that forms prominences from any part of the tachyzoite [98].

The success of *T. gondii* tachyzoites as intracellular parasites is indicated by utilizing the infected host cell to serve their nutritional needs, this is conferred by a well-developed tubulovesicular network and the trafficking of the host's mitochondria and endoplasmic reticulum around the PVs. Upon treatment with SeNPs, the latter features were deranged, with overall haziness of the membranes and organelles' boundaries; features that could be explained by the deficiency of essential nutrients such as amino acids, phospholipids, folates, and fatty acids required by the parasite to release essential recruitment proteins to control host's organelles [101]. These ultrastructural changes can explain the drop in parasite tissue load which mirrors the loss of invasiveness, virulence, and reproduction of the parasite upon treatment.

There was an obvious attraction of SeNPs to the outer membrane components of the tachyzoites which was confirmed by SEM. In addition, the trafficking of SeNPs molecules into the tachyzoites was demonstrated by TEM. The presence of the nanosized particles inside the cytoplasmic vacuoles might indicate their possible penetration to the nuclei and their binding with the parasite DNA. They may have led to

changes in tachyzoites morphology, cell wall integrity, and permeability. Some of the observed morphological changes in this study were previously associated with apoptosis. Tachyzoites showed signs of degradation with extensive clefts, vacuoles, and membrane blebs. The extensive lysis of the cytoplasm was especially noticed around the nucleus and in the area of the apical complex. Similar changes were noticed by Portes et al. [102] who reported that after 6 days of *Toxoplasma* treatment with dinuclear iron compound, the tachyzoites exhibited ultrastructural alterations suggestive of apoptosis. Their SEM and TEM analyses revealed extensive cytoplasmic clefts and the appearance of blebs in the parasite membrane, which are hallmarks of undergoing apoptotic cell death. Moreover, Giovati et al. [103] observed the apoptotic changes in killer peptide-treated tachyzoites which included cytoplasmic vacuolation, blurring of conoid, disruption of the nuclear membrane, and chromatin condensation.

Other important observed alterations in the SeNPs-treated group include degenerated nuclear membrane, absence of nucleolus, and halo mark around the nucleus with multiple dense chromatin granules inside the nucleus. It was proposed that a key event of apoptosis is endonucleolysis, which results in the cleavage of nuclear DNA into oligonucleosome-sized fragments [104]. The observation of condensed chromatin has been demonstrated to consist of endogenously digested chromatin fragments in mammalian apoptotic cells [105].

Another key underlying mechanism of the anti-*T. gondii* activity of SeNps could be a proposed effect on the oxidation-reduction process of the parasite which may in turn lead to autophagy. The latter is manifested by the appearance of autophagic vacuoles in the cytoplasm, nuclear degeneration, and the disintegration of the parasite gradually. Zhang et al. [106] suggested that myrislignan (originated from nutmeg) may affect the oxidation-reduction process of *T. gondii* leading to autophagy and subsequently causing *T. gondii* tachyzoites death. At first, it caused many autophagic vacuoles to emerge in the cytoplasm. Then, the cytoplasmic structure and PV membranes of tachyzoites completely disappeared, and progressive degeneration of the parasites was detected. Similar changes were observed after licarin-B treatment which induced an autophagy-like double membrane structure, cytoplasmic vacuoles, and nuclear disintegration in *T. gondii* tachyzoites [107].

All of the previous features were evident in treated groups of the present study suggesting the simultaneous occurrence of different types of cell death by the parasite upon treatment. Interestingly, the simultaneous occurrence of different types of cell death, such as autophagy, apoptosis, and necrosis has been described in other parasites such as *T. cruzi* [108] and

Leishmania infantum [109]. Most importantly, this phenomenon has been observed in *T. gondii* after treatment with the dinuclear iron compound where both autophagy and apoptosis occurred [102]. Moreover, Machado et al. [110] suggested that the parasite may die via different mechanisms after treatment with the antioxidant melatonin where *T. gondii* showed signs of necrotic cell death as well as apoptotic cell death. The existence of apoptotic and autophagic changes in the present study suggests that both cell death mechanisms could be encountered with SeNPs treatment.

To our knowledge the present work provides the first reports on the therapeutic effects of biologically synthesized selenium nanoparticles on acute toxoplasmosis caused by virulent-RH strain of *Toxoplasma gondii*, as previous studies by Keyhani et al. [30; 31] and Shakibaie et al. [111] investigated the effects of selenocompounds on chronic toxoplasmosis and their prophylactic effects on acute toxoplasmosis respectively. Moreover, our study emphasized in-depth that ultrastructural changes of the treated parasite hypothesized the mechanism of action of selenium nanoparticles including the apoptotic mechanism and autophagy signs as demonstrated in transmission electron microscopic study.

The present study proves that SeNps can provide a reliable natural alternative anti-*Toxoplasma* agent in conditions where side effects and drug toxicity issues emerge as unsolved problems in routine drug regimens. It further emphasized the possible mechanisms of parasite killing with selenocompounds as apoptosis and autophagy. The antioxidant effect of selenocompounds in acute toxoplasmosis was also elucidated. However, further studies are to be carried out to test the efficacy and side effects of other trace elements as anti-protozoal agents.

Disclosure statement

No potential conflict of interest was reported by the author(s).

Funding

The author(s) reported there is no funding associated with the work featured in this article.

References

- [1] Dupont CD, Christian DA, Hunter CA. Immune response and immunopathology during toxoplasmosis. *Semin Immunopathol.* 2012;34(6):793–813.
- [2] Szewczyk-Golec K, Pawlowska M, Wesolowski R, et al. Oxidative stress as a possible target in the treatment of toxoplasmosis: perspectives and ambiguities. *Int J Mol Sci.* 2021;22(11):5705.
- [3] Jones JL, Kruszon-Moran D, Wilson M, et al. *Toxoplasma gondii* infection in the United States:

- seroprevalence and risk factors. *Am J Epidemiol.* **2001**;154(4):357–365.
- [4] Hill DE, Dubey JP. *Toxoplasma gondii* as a parasite in food: analysis and control. *Microbiol Spectr.* **2016**;4(4). DOI:10.1128/microbiolspec.PFS-0011-2015
- [5] Magaña-López R, Zaragoza-Sánchez PI, Jiménez-Cisneros BE, et al. The use of TiO₂ as a disinfectant in water sanitation applications. *Water.* **2021**;13(12):1641.
- [6] Converse RR, Wade TJ, Krueger Ws, Hilborn Ed. Drinking water source and human *Toxoplasma gondii* infection in the United States: a cross-sectional analysis of NHANES data. *BMC Public Health.* **2014**;14(1):711. DOI:10.1186/1471-2458-14-711
- [7] Konstantinovic N, Guegan H, Stajner T, et al. Treatment of toxoplasmosis: current options and future perspectives. *Food Waterborne Parasitol.* **2019**;15:e00036.
- [8] Silva LA, Reis-Cunha JL, Bartholomeu DC, et al. Genetic polymorphisms and phenotypic profiles of sulfadiazine-resistant and sensitive *Toxoplasma gondii* isolates obtained from newborns with congenital toxoplasmosis in Minas Gerais, Brazil. *PLoS ONE.* **2017**;12(1):e0170689.
- [9] Eltarahony M, Abu-Serie M, Hamad H, et al. Unveiling the role of novel biogenic functionalized CuFe hybrid nanocomposites in boosting anticancer, antimicrobial and biosorption activities. *Sci Rep.* **2021a**;11(1):7790.
- [10] Elyamny S, Eltarahony M, Abu-Serie M, et al. One-pot fabrication of Ag @ag₂O core-shell nanostructures for biosafe antimicrobial and antibiofilm applications. *Sci Rep.* **2021**;11(1):22543.
- [11] Zaki SA, Eltarahony MM, Abd-El-Haleem DA. Disinfection of water and wastewater by biosynthesized magnetite and zerovalent iron nanoparticles via NAP-NAR enzymes of *Proteus mirabilis* 10B. *Environ Sci Pollut Res Int.* **2019**;26(23):23661–23678.
- [12] Eltarahony M, Zaki S, Abd-El-Haleem D. Concurrent synthesis of zero- and one-dimensional, spherical, rod-, needle-, and wire-shaped CuO nanoparticles by *Proteus mirabilis* 10B. *J Nanomater.* **2018a**;2018:1849616.
- [13] Martínez-Esquivias F, Guzmán-Flores JM, Pérez-Larios A, et al. A review of the antimicrobial activity of selenium nanoparticles. *J Nanosci Nanotechnol.* **2021**;21(11):5383–5398.
- [14] Singh P, Kim YJ, Zhang D, et al. Biological synthesis of nanoparticles from plants and microorganisms. *Trends Biotechnol.* **2016**;34(7):588–599.
- [15] Zhang D, Ma XL, Gu Y, et al. Green synthesis of metallic nanoparticles and their potential applications to treat cancer. *Front Chem.* **2020**;8:799.
- [16] Manimaran M, Kannabiran K. Actinomycetes-mediated biogenic synthesis of metal and metal oxide nanoparticles: progress and challenges. *Lett Appl Microbiol.* **2017**;64(6):401–408.
- [17] Eltarahony M, Ibrahim A, El-Shall H, et al. Antibacterial, antifungal and antibiofilm activities of silver nanoparticles supported by crude bioactive metabolites of bionanofactories isolated from lake mariout. *Molecules.* **2021b**;26(10):3027.
- [18] Eltarahony M, Zaki S, Elkady M, et al. Biosynthesis, characterization of some combined nanoparticles, and its biocide potency against a broad spectrum of pathogens. *J Nanomater.* **2018b**;2018:5263814.
- [19] Chandrakala V, Aruna V, Angajala G. Review on metal nanoparticles as nanocarriers: current challenges and perspectives in drug delivery systems. *Emergent Mater.* **2022**;5(6):1–23.
- [20] Thanki K, Gangwal RP, Sangamwar AT, et al. Oral delivery of anticancer drugs: challenges and opportunities. *J Control Release.* **2013**;170(1):15–40.
- [21] Klębowski B, Depciuch J, Parlińska-Wojtan M, et al. Applications of noble metal-based nanoparticles in medicine. *Int J Mol Sci.* **2018**;19(12):4031.
- [22] Rayman MP. Selenium and human health. *Lancet.* **2012**;379(9822):1256–1268.
- [23] Naithani R. Organoselenium compounds in cancer chemoprevention. *Mini Rev Med Chem.* **2008**;8(7):657–668.
- [24] Hariharan S, Dharmaraj S. Selenium and selenoproteins: it's role in regulation of inflammation. *Inflammopharmacology.* **2020**;28(3):667–695.
- [25] Alkudhayri A, Al-Shaebi EM, Qasem MAA, et al. Antioxidant and anti-apoptotic effects of selenium nanoparticles against murine eimeriosis. *Anais da Academia Brasileira de Ciências.* **2020**;92(2):e20191107.
- [26] Barbosa CF, Tonin AA, Da Silva AS, et al. Diphenyl diselenide and sodium selenite associated with chemotherapy in experimental toxoplasmosis: influence on oxidant/antioxidant biomarkers and cytokine modulation. *Parasitology.* **2014**;141(13):1761–1768.
- [27] Yetisgin AA, Cetinel S, Zuvun M, et al. Therapeutic nanoparticles and their targeted delivery applications. *Molecules.* **2020**;25(9):2193.
- [28] Ikram M, Javed B, Raja NI, et al. Biomedical potential of plant-based selenium nanoparticles: a comprehensive review on therapeutic and mechanistic aspects. *Int J Nanomed.* **2021**;16:249–268.
- [29] Martínez-Esquivias F, Gutiérrez-Angulo M, Pérez-Larios A, et al. Anticancer activity of selenium nanoparticles *in vitro* studies. *Anticancer Agents Med Chem.* **2022**;22(9):1658–1673.
- [30] Keyhani A, Shakibaie M, Mahmoudvand H, et al. Prophylactic activity of biogenic selenium nanoparticles against chronic *Toxoplasma gondii* infection. *Recent Pat Antiinfect Drug Discov.* **2020a**;15(1):75–84.
- [31] Keyhani A, Ziaali N, Shakibaie M, et al. Biogenic selenium nanoparticles target chronic toxoplasmosis with minimal cytotoxicity in a mouse model. *J Med Microbiol.* **2020b**;69(1):104–110.
- [32] Krishnan M, Ranganathan K, Maadhu P, et al. Leaf extract of *dillenia indica* as a source of selenium nanoparticles with larvicidal and antimicrobial potential toward vector mosquitoes and pathogenic microbes. *Coatings.* **2020**;10(7):626.
- [33] El-Tombary AA, Ismail KA, Aboulwafa OM, et al. Novel triazolo[4,3-a]quinazolinone and bis-triazolo[4,3-a:4,3'-c]quinazolines: synthesis and antitoxoplasmosis effect. *Farmacol.* **1999**;54(7):486–495.
- [34] Nair AB, Jacob S. A simple practice guide for dose conversion between animals and human. *J Basic Clin Pharm.* **2016**;7(2):27–31.
- [35] Eissa MM, Barakat AM, Amer EI, et al. Could miltefosine be used as a therapy for toxoplasmosis? *Exp Parasitol.* **2015**;157:12–22.
- [36] Wang Y, Wang M, Wang G, et al. Increased survival time in mice vaccinated with a branched lysine multiple antigenic peptide containing B- and T-cell epitopes from *T. gondii* antigens. *Vaccine.* **2011**;29(47):8619–8623.
- [37] Al Dakhil MA, Morsy TA. Natural *Toxoplasma* infection sought in the Indian grey mongoose (*H. edwardsi*,

- Greffroy, 1818) trapped in the eastern region., Saudi Arabia. *J Egypt Soc Parasitol.* 1996;26(3):645–652.
- [38] Abou-El-Naga IF, El Kerdany ED, Mady RF, et al. The effect of lopinavir/ritonavir and lopinavir/ritonavir loaded PLGA nanoparticles on experimental toxoplasmosis. *Parasitol Int.* 2017;66(6):735–747.
- [39] Klainer AS, Betsch CJ. Scanning-beam electron microscopy of selected microorganisms. *J Infect Dis.* 1970;121(3):339–343.
- [40] Trachootham D, Lu W, Ogasawara MA, et al. Redox regulation of cell survival. *Antioxid Redox Signal.* 2008;10(8):1343–1374.
- [41] Koracevic D, Koracevic G, Djordjevic V, et al. Method for the measurement of antioxidant activity in human fluids. *J Clin Pathol.* 2001;54(5):356–361.
- [42] Alsamhary KI. Eco-friendly synthesis of silver nanoparticles by *Bacillus subtilis* and their antibacterial activity. *Saudi J Biol Sci.* 2020;27(8):2185–2191.
- [43] Nirmala C, Sridevi M. Characterization, antimicrobial and antioxidant evaluation of biofabricated silver nanoparticles from endophytic *Pantoea anthophila*. *J Inorg Organomet Polym Mater.* 2021;31(9):3711–3725.
- [44] Zain N, Kadir M. The stabilisation of calcium carbonate vaterite phase via integration of mussel-inspired polydopamine. *Inter Med Dev Technol Conf.* 2017;203–206.
- [45] Kemel K, Baillet-Guffroy A, Faivre V, et al. ATR-FTIR characterization of Janus nanoparticles—part II: follow-up skin application. *J Pharm Sci.* 2019;108(10):3366–3371.
- [46] Qi W, Tian Y, Lu D, et al. Detection of glutathione in dairy products based on surface-enhanced infrared absorption spectroscopy of silver nanoparticles. *Front Nutr.* 2022;9:982228.
- [47] Jyoti K, Baunthiyal M, Singh A. Characterization of silver nanoparticles synthesized using *Urtica dioica* Linn. leaves and their synergistic effects with antibiotics. *J Radiat Res Appl Sci.* 2016;9(3):217–227.
- [48] Nalbandian L, Patrikiadou E, Zaspalis V, et al. Magnetic nanoparticles in medical diagnostic applications: synthesis, characterization and proteins conjugation. *Curr Nanosci.* 2016;12(4):455–468.
- [49] Royji Albeladi SS, Malik MA, Al-Thabaiti SA. Facile bio-fabrication of silver nanoparticles using *Salvia officinalis* leaf extract and its catalytic activity towards Congo red dye degradation. *J Mater Sci Technol.* 2020;9(5):10031–10044.
- [50] Lian S, Diko CS, Yan Y, et al. Characterization of biogenic selenium nanoparticles derived from cell-free extracts of a novel yeast *Magnusiomyces ingens*. *3 Biotech.* 2019;9(6):221.
- [51] Tugarova AV, Mamchenkova PV, Dyatlova YA, et al. FTIR and Raman spectroscopic studies of selenium nanoparticles synthesized by the bacterium *Azospirillum thioophilum*. *Spectrochim Acta A Mol Biomol Spectrosc.* 2018;192:458–463.
- [52] Bharathi S, Kumaran S, Suresh G, et al. Extracellular synthesis of nanoselenium from fresh water bacteria *Bacillus sp.*, and its validation of antibacterial and cytotoxic potential. *Biocatal Agric Biotechnol.* 2020;27:101655.
- [53] Hassan SE, Fouda A, Radwan AA, et al. Endophytic actinomycetes *Streptomyces spp* mediated biosynthesis of copper oxide nanoparticles as a promising tool for biotechnological applications. *J Biol Inorg Chem.* 2019;24(3):377–393.
- [54] Al Jahdaly BA, Al-Radadi NS, Eldin GMG, et al. Selenium nanoparticles synthesized using an eco-friendly method: dye decolorization from aqueous solutions, cell viability, antioxidant, and antibacterial effectiveness. *J Mater Res Technol.* 2021;11:85–97.
- [55] Andrews KT, Fisher G, Skinner-Adams TS. Drug repurposing and human parasitic protozoan diseases. *Int J Parasitol Drugs Drug Resist.* 2014;4(2):95–111.
- [56] Antczak M, Dzitko K, Dlugonska H. Human toxoplasmosis—searching for novel chemotherapeutics. *Biomed Pharmacother.* 2016;82:677–684.
- [57] Masters PA, O'bryan TA, Zurlo J, et al. Trimethoprim-sulfamethoxazole revisited. *Arch Intern Med.* 2003;163(4):402–410.
- [58] Kim JH, Lee J, Bae SJ, et al. NADPH oxidase 4 is required for the generation of macrophage migration inhibitory factor and host defense against *Toxoplasma gondii* infection. *Sci Rep.* 2017;7(1):6361.
- [59] Khan I, Saeed K, Khan I. Nanoparticles: properties, applications and toxicities. *Arab J Chem.* 2019a;12(7):908–931.
- [60] Gawande MB, Goswami A, Felpin F-X, et al. Cu and Cu-based nanoparticles: synthesis and applications in catalysis. *Chem Rev.* 2016;116(6):3722–3811.
- [61] Shar AH, Lakhani MN, Wang J, et al. Facile synthesis and characterization of selenium nanoparticles by the hydrothermal approach. *Dig J Nanomater Nanostructures.* 2019;14:867–872.
- [62] Vahdati M, Tohidi Moghadam T. Synthesis and characterization of selenium nanoparticles-lysozyme nano-hybrid system with synergistic antibacterial properties. *Sci Rep.* 2020;10(1):510.
- [63] Cittrarasu V, Kaliannan D, Dharman K, et al. Green synthesis of selenium nanoparticles mediated from *Ceropegia bulbosa* Roxb extract and its cytotoxicity, antimicrobial, mosquitocidal and photocatalytic activities. *Sci Rep.* 2021;11(1):1032.
- [64] Abu-Serie MM, Eltarahony M. Novel nanoformulated diethyldithiocarbamate complexes with biosynthesized or green chemosynthesized copper oxide nanoparticles: an in vitro comparative anticancer study. *Int J Pharm.* 2021;609:121149.
- [65] Ur Rahman SS, Qureshi MT, Sultana K, et al. Single step growth of iron oxide nanoparticles and their use as glucose biosensor. *Results Phys.* 2017;7:4451–4456.
- [66] Geoffrion LD, Hesabizadeh T, Medina-Cruz D, et al. Naked selenium nanoparticles for antibacterial and anticancer treatments. *ACS Omega.* 2020;5(6):2660–2669.
- [67] Filipovic N, Usjak D, Milenkovic MT, et al. Comparative study of the antimicrobial activity of selenium nanoparticles with different surface chemistry and structure. *Front Bioeng Biotechnol.* 2020;8:624621.
- [68] Sathyanarayanan MB, Balachandranath R, Genji Srinivasulu Y, et al. The effect of gold and iron-oxide nanoparticles on biofilm-forming pathogens. *ISRN Microbiol.* 2013;2013:272086.
- [69] Venditti I, Hassanein T, Fratoddi I, et al. Bioconjugation of gold-polymer core-shell nanoparticles with bovine serum amine oxidase for biomedical applications. *Colloids Surf B Biointerfaces.* 2015;134:314–321.
- [70] Saeb AT, Alshammari AS, Al-Brahim H, et al. Production of silver nanoparticles with strong and stable antimicrobial activity against highly pathogenic and multidrug resistant bacteria. *Sci World J.* 2014;2014:704708.

- [71] Pyrzynska K, Sentkowska A. Biosynthesis of selenium nanoparticles using plant extracts. *J Nanostruct Chem.* **2022**;12(4):467–480.
- [72] Ullah A, Yin X, Wang F, et al. Biosynthesis of selenium nanoparticles (via *Bacillus subtilis* BSN313), and their isolation, characterization, and bioactivities. *Molecules.* **2021**;26(18):5559.
- [73] Ren L, Wu Z, Ma Y, et al. Preparation and growth-promoting effect of selenium nanoparticles capped by polysaccharide-protein complexes on tilapia. *J Sci Food Agric.* **2021**;101(2):476–485.
- [74] Kieliszek M, Blazejak S. Current knowledge on the importance of selenium in food for living organisms: a review. *Molecules.* **2016**;21(5):609.
- [75] Mostofa MG, Hossain MA, Siddiqui MN, et al. Phenotypical, physiological and biochemical analyses provide insight into selenium-induced phytotoxicity in rice plants. *Chemosphere.* **2017**;178:212–223.
- [76] Selvaraj V, Yeager-Armstead M, Murray E. Protective and antioxidant role of selenium on arsenic trioxide-induced oxidative stress and genotoxicity in the fish hepatoma cell line PLHC-1. *Environ Toxicol Chem.* **2012**;31(12):2861–2869.
- [77] Guillin OM, Vindry C, Ohlmann T, et al. Selenium, selenoproteins and viral infection. *Nutrients.* **2019**;11(9):2101.
- [78] Khan IA, Hwang S, Moretto M. *Toxoplasma gondii*: cD8 T cells cry for CD4 help. *Front Cell Infect Microbiol.* **2019b**;9:136.
- [79] Bae M, Kim H. Mini-review on the roles of vitamin c, vitamin d, and selenium in the immune system against COVID-19. *Molecules.* **2020**;25(22):5346.
- [80] Hawkes WC, Kelley DS, Taylor PC. The effects of dietary selenium on the immune system in healthy men. *Biol Trace Elem Res.* **2001**;81(3):189–213.
- [81] Hoffmann FW, Hashimoto AC, Shafer LA, et al. Dietary selenium modulates activation and differentiation of CD4+ T cells in mice through a mechanism involving cellular free thiols. *J Nutr.* **2010**;140(6):1155–1161.
- [82] Wood SM, Beckham C, Yosioka A, et al. β -Carotene and selenium supplementation enhances immune response in aged humans. *Integr Med.* **2000**;2(2–3):85–92.
- [83] Burk RF, Hill KE. Regulation of selenium metabolism and transport. *Annu Rev Nutr.* **2015**;35(1):109–134.
- [84] Lu J, Holmgren A. Selenoproteins. *J Biol Chem.* **2009**;284(2):723–727.
- [85] Lu J, Holmgren A. The thioredoxin antioxidant system. *Free Radic Biol Med.* **2014**;66:75–87.
- [86] Xue J, Jiang W, Chen Y, et al. Thioredoxin reductase from *Toxoplasma gondii*: an essential virulence effector with antioxidant function. *Faseb J.* **2017**;31(10):4447–4457.
- [87] Elsheikha HM, El-Motayam MH, Abouel-Nour MF, et al. Oxidative stress and immune-suppression in *Toxoplasma gondii* positive blood donors: implications for safe blood transfusion. *J Egypt Soc Parasitol.* **2009**;39(2):421–428.
- [88] Machado VS, Bottari NB, Baldissera MD, et al. Diphenyl diselenide supplementation in infected mice by *Toxoplasma gondii*: protective effect on behavior, neuromodulation and oxidative stress caused by disease. *Exp Parasitol.* **2016**;169:51–58.
- [89] Khaleel FM, Hameed AS, Dawood AS. Evaluation of antioxidant (GSH, vitamin A, E, C) and MDA in Iraqi women with toxoplasmosis. *Indian J Forensic Med Toxicol.* **2020**;14:1446–1449.
- [90] Kalantari P, Narayan V, Natarajan SK, et al. Thioredoxin reductase-1 negatively regulates HIV-1 transactivating protein Tat-dependent transcription in human macrophages. *J Biol Chem.* **2008**;283(48):33183–33190.
- [91] Sheridan PA, Zhong N, Carlson BA, et al. Decreased selenoprotein expression alters the immune response during influenza virus infection in mice. *J Nutr.* **2007**;137(6):1466–1471.
- [92] Arthur JR, McKenzie RC, Beckett GJ. Selenium in the immune system. *J Nutr.* **2003**;133(5):1457S–1459S.
- [93] Forman HJ, Torres M. Reactive oxygen species and cell signaling: respiratory burst in macrophage signaling. *Am J Respir Crit Care Med.* **2002**;166(supplement_1):S4–8.
- [94] Black MW, Boothroyd JC. Lytic cycle of *Toxoplasma gondii*. *Microbiol Mol Biol Rev.* **2000**;64(3):607–623.
- [95] Morrisette NS, Sibley LD. Cytoskeleton of apicomplexan parasites. *Microbiol Mol Biol Rev.* **2002**;66(1):21–38.
- [96] Rivera Fernández N, Mondragón Castelán M, González Pozos S, et al. A new type of quinoxalinone derivatives affects viability, invasion, and intracellular growth of *Toxoplasma gondii* tachyzoites in vitro. *Parasitol Res.* **2016**;115(5):2081–2096.
- [97] FarahatAllam A, Shehab AY, Fawzy Hussein Mogahed NM, et al. Effect of nitazoxanide and spiramycin metronidazole combination in acute experimental toxoplasmosis. *Heliyon.* **2020**;6(4):e03661.
- [98] de Leon JC, Scheumann N, Beatty W, et al. A SAS-6-like protein suggests that the *Toxoplasma* conoid complex evolved from flagellar components. *Eukaryot Cell.* **2013**;12(7):1009–1019.
- [99] Hammouda NA, El-Mansoury ST, El-Azzouni MZ. *Toxoplasma gondii*: scanning electron microscopic study before and after treatment. *J Trop Med.* **1992**;2:77–83.
- [100] Gaafar MR, Mady RF, Diab RG, et al. Chitosan and silver nanoparticles: promising anti-*toxoplasma* agents. *Exp Parasitol.* **2014**;143:30–38.
- [101] Hammoudi PM, Jacot D, Mueller C, et al. Fundamental roles of the golgi-associated *Toxoplasma* Aspartyl Protease, ASP5, at the host-parasite interface. *PLOS Pathog.* **2015**;11(10):e1005211.
- [102] Portes JA, Souza TG, dos Santos TA, et al. Reduction of *Toxoplasma gondii* development due to inhibition of parasite antioxidant enzymes by a dinuclear Iron(III) compound. *Antimicrob Agents Chemother.* **2015**;59(12):7374–7386.
- [103] Giovati L, Santinoli C, Mangia C, et al. Novel activity of a synthetic decapeptide against *Toxoplasma gondii* Tachyzoites. *Front Microbiol.* **2018**;9:753.
- [104] Elmore S. Apoptosis: a review of programmed cell death. *Toxicol Pathol.* **2007**;35(4):495–516.
- [105] Wyllie AH, Morris RG, Smith AL, et al. Chromatin cleavage in apoptosis: association with condensed chromatin morphology and dependence on macromolecular synthesis. *J Pathol.* **1984**;142(1):67–77.
- [106] Zhang J, Chen J, Lv K, et al. Myrislignan induces redox imbalance and activates autophagy in *Toxoplasma gondii*. *Front Cell Infect Microbiol.* **2021a**;11:730222.

- [107] Zhang J, Si H, Lv K, et al. Licarin-B exhibits activity against the *Toxoplasma gondii* RH strain by damaging mitochondria and activating autophagy. *Front Cell Dev Biol.* [2021b](#);9:684393.
- [108] Menna-Barreto RF, Salomao K, Dantas AP, et al. Different cell death pathways induced by drugs in *Trypanosoma cruzi*: an ultrastructural study. *Micron.* [2009](#);40(2):157–168.
- [109] Abou-El-Naga IF, Mady RF, Fawzy Hussien Mogahed NM. In vitro effectivity of three approved drugs and their synergistic interaction against *Leishmania infantum*. *Biomédica.* [2020](#);40(Supl. 1):89–101.
- [110] Machado NI, Dos Santos TAT, de Souza W, et al. Treatment with melatonin induces a reduction of *Toxoplasma gondii* development in LLC-MK2 cells. *Parasitol Res.* [2020](#);119(8):2703–2711.
- [111] Shakibaie M, Ezzatkah F, Gabal E, et al. Prophylactic effects of biogenic selenium nanoparticles on acute toxoplasmosis: an in vivo study. *Ann Med Surg (Lond).* [2020](#);54:85–88.